Soft Matter

Charge regulation mechanism in end-tethered weak polyampholytes

Journal:	*Soft Matter*
Manuscript ID	SM-ART-07-2020-001323.R1
Article Type:	Paper
Date Submitted by the Author:	29-Aug-2020
Complete List of Authors:	Prusty, Debadutta; Northwestern University, Materials Science and Engineering Nap, Rikkert; Northwestern University, Department of Biomedical Engineering Szleifer, Igal; Northwestern University, Department of Biomedical Engineering Olvera de la Cruz, Monica; Northwestern University, Materials Science and Engineering

Soft Matter

ARTICLE TYPE

Cite this: DOI: 00.0000/xxxxxxxxxx

Charge regulation mechanism in end-tethered weak polyampholytes†

D. Prusty[a], R.J. Nap [b,c], I. Szleifer [b,c,d] and M. Olvera de la Cruz[a,d,e‡]

Received Date
Accepted Date

DOI: 00.0000/xxxxxxxxxx

Weak polyampholytes, containing oppositely charged dissociable groups, are expected to be responsive to changes in ionic conditions. Here, we determine structural and thermodynamic properties, including the charged groups' degrees of dissociation, of end-tethered weak polyampholyte layers as a function of salt concentration, pH, and the solvent quality. For diblock weak polyampholytes grafted by their acidic blocks, we find that the acidic monomers increase their charge while the basic monomers decrease their charge with decreasing salt concentration for pH values less than the pKa value of both monomers and vice versa when the pH > pKa. This complex charge regulation occurs because the electrostatic attraction between oppositely charged blocks is stronger than the repulsion between monomers with the same charge in both good and poor solvents when the screening by salt ions is weak. This is evidenced by the retraction of the top block into the bottom layer. In the case of poor solvent conditions to the basic block (the top block), we find lateral segregation of basic monomers into micelles, forming a two-dimensional hexagonal pattern on the surface at intermediate and high pH values for monovalent salt concentrations from 0.01 to 0.1 M. When the solvent is poor to both blocks, we find lateral segregation of the grafted acidic block into lamellae with longitudinal undulations of low and high acidic monomer density. By exploiting weak block polyampholytes, our work expands the parameter space for creating responsive surfaces stable over a wide range of pH and salt concentration.

1 Introduction

End-tethered polymers, also known as polymer brushes, are ubiquitous in applications involving surface modification, such as colloidal and nanoparticle stabilization[1–3] and surface lubrication[4,5]. More recently, they have also become the subject of intense theoretical and experimental investigation for potential nano-technological and biomedical applications[6]. For example, polymer modified nanopores show promise in applications such as water purifaction[7], nanofluidic circuits[8,9], and chemical sensing[10,11]. Likewise, polymer tethered colloids and nanoparticles have biomedical applications that include usages as drug delivery devices[12,13] and contrast agents[14,15].

The morphology of the polymer brushes in these applications dictates the coating performance. Hence, understanding the formation of the surface patterns and external factors that control them is of key importance. Among different types of brushes, particularly interesting are end-tethered weak polyelectrolytes, since here, the presence of chargeable monomers and their dissociation behavior provides structural control through adjustments in pH and salt concentration, in addition to conventional thermal responsiveness through solvent-polymer interactions[16]. In contrast to an end-tethered strong polyelectrolyte, where charges on the polymer chains are fixed, end-tethered weak polyelectrolytes change their degree of charge in response to external cues such as pH, salt concentration, and the grafting density. This provides greater control over the tunability of the structural and thermodynamic properties of the brush, as well as switchability between various surface patterns[17,18].

Prior work on end-tethered polymers has focused on both single-component and multi-component brushes. The latter are more interesting since the interplay of more interactions can broaden the set of possible microphase separated structures[19–21], such as in block copolymer brushes[22–24]. The difference in solvent selectivity between the components as well as the relative composition of the polymers induces various surface patterns such as spherical micelles,stripes, worm-like micelles, and holes[23,25]. Furthermore, in the case of binary polyelectrolyte

[a] Department of Materials Science and Engineering, Northwestern University, Evanston, Illinois 60208, United States
[b] Department of Biomedical Engineering, Northwestern University, Evanston, Illinois 60208, United States
[c] Chemistry of Life Processes Institute, Northwestern University, Evanston, Illinois 60208, United States
[d] Department of Chemistry, Northwestern University, Evanston, Illinois 60208, United States
[e] Department of Physics and Astronomy, Northwestern University, Evanston, Illinois 60208, United States

† Electronic Supplementary Information (ESI) available: [details of any supplementary information available should be included here]. See DOI: 10.1039/cXsm00000x/

‡ m-olvera@northwestern.edu

brushes with both monomers capable of dissociation, greater control on morphology tuning can be achieved by varying the pH and salt concentration[26–28]. However, unlike their neutral counterparts, where there have been extensive theoretical as well as experimental investigations, multi-component polyelectrolyte brushes have received far less attention in theoretical studies.

For example, Meng and Wang[29] used 1D self-consistent field theory (SCFT) to study the solvent response of a diblock copolymer brush with one of its blocks strongly charged as a function of the solvent selectivity, the charge fraction of the charged block and an externally imposed electric field. The authors observed that the efficacy of the relative solvent selectivity towards blocks in switching the surface composition drops with increasing charge fraction as electrostatic effects become more dominant than the Van der Waals repulsion. Structural transitions were indeed observed when the charged block was made weakly chargeable. However, the degree of dissociation was considered to be constant and independent of monomer position as well as salt concentration. The degree of charging was set by the pH of the reservoir, using the Henderson-Hasselbalch equation for acids in dilute solution. However, as the theoretical work by Israëls and coworkers[30–32] and other subsequent investigations[33] have already demonstrated, the degree of dissociation of a monomer in a polyacid brush is strongly dependent on its location within the polymer layer. Thus, the monomer dissociation in a brush can be drastically different from the extent of charging of the same acidic-group in solution, as was also observed experimentally[18]. The monomer dissociation behavior is also strongly influenced by grafting density and salt concentration[33,34].

Another example of a theoretical investigation involving end-grafted polyampholytes involves a study by Shusharina and Linse[35,36], which used the mean-field lattice theory developed by Scheutjens and Fleer[37] to study the density profiles of oppositely charged strong diblock and mixed polyelectrolyte brushes. They found that the opposite charges result in a cancellation of the electrostatic interactions, causing the system to behave as a neutral brush. This cancellation is accompanied by a change in the conformation distribution of polymer chains. Similar theoretical and simulation-based studies have been performed on polyampholyte brushes with either both blocks having fixed charges or one block having pH-responsive monomers[38–40].

In this work, we develop a molecular theory to study the structure and thermodynamic behavior of weakly chargeable end-tethered polyampholytes for several different sequences of acidic and basic monomers. The Molecular Theory has been used in the past to predict the behavior of a variety of end-tethered polymeric systems including neutral polymers as well as polyelectrolytes[41]. The predictions of the theory are in good agreement with experimental observations. For example, predictions of the height of poly(acrylic acid) (PAA) brushes and the charge of acid-ligated gold nanoparticles are consistent with experimental measurements[42,43]. The theoretical approach takes into account the size, shape, conformation, and charge distribution of each molecular species. It includes the conformations of the polymers explicitly and considers the acid–base equilibrium of each acidic and basic group of the polyelectrolyte. The basic idea of this detailed molecular theory is to express the free energy functional of the system in terms of the density distributions of all species and the probability distribution of the polymer conformations. The minimization of the total free energy determines the equilibrium density distribution of all molecular components, the probability of the different conformations, the electrostatic and repulsive position-dependent potentials, as well as the chemical state of every species[44,45]. Thus, importantly, the chemical state is not imposed, instead, it follows from free energy minimization. A similar approach has been used in the past by Yethiraj and Woodward[46] for polymer melts confined between flat plates. There, a single polymer chain is subjected to the field coming from the classical density functional theory and then the polymer density is obtained by taking the average over all polymer configurations through a Monte-Carlo method. In our work, we apply the molecular theory to a polymer brush with both acidic and basic chargeable groups. Examples of acidic and basic groups are carboxylic acid and 2-vinyl pyridine, which, depending on pH, can acquire a negative or a positive charge, respectively. We study the dissociation behavior of these groups as a function of pH at various salt concentrations, surface grafting densities, and polymer sequences.

Besides pH and salt, the degree of charging is also affected by the density of the layers. The polymer density in the layer is also controlled by grafting density and solvent-quality. Non-electrostatic attractions between the monomers, the strengths of which are reflected in the solvent quality, can result in an increased density or even collapse of the polymer brush. Hence, we also investigate the coupling between the degree of dissociation of the acidic and basic monomers of the polymer brush and solvent quality.

In Section 2, we describe the weak polyampholyte brushes model and discuss the different contributions to the total free energy. This is followed by a discussion of our results. Specifically, in Section 3.1, we determine the dependence of the degree of charging of monomers on pH and salt; we show that the upper block is more sensitive to the salt concentration than the lower one due to conformational entropy of the chain. In Section 3.2, we find that the variation of the height of the brush with pH is a non-monotonic function of salt. In Section 3.3, we evaluate the lateral stability of the brush under poor solvent conditions by investigating the chemical potential of the polymer at different grafting densities. This one dimensional analysis is complemented by full three dimensional calculations on the brush. For solvents poor to the upper block, we find phase separation of the brush into micelles of the basic monomers "floating" on top of the homogeneous acidic layer at high and intermediate pH values. When the solvent is poor to both blocks, we find undulated lamellar structures of grafted acidic monomers engulfed by basic monomers at low pH values. At high pH values, however, we find a micellar phase of basic monomers on a homogeneous layer of acidic grafted monomer. Finally, in section 4, we present conclusions and discuss potential future directions.

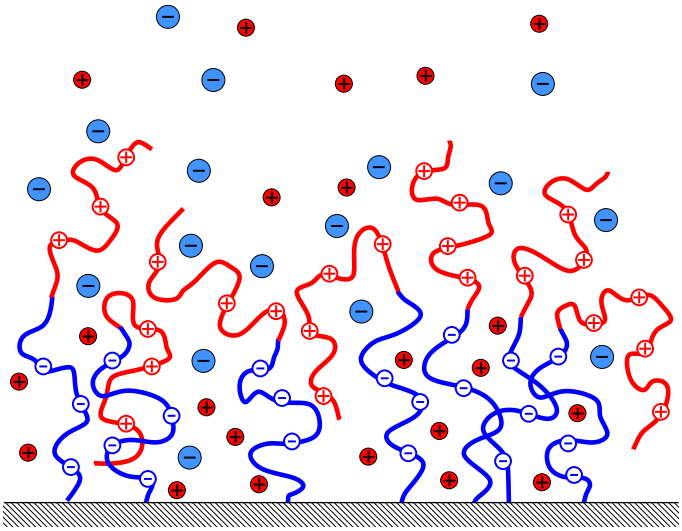

Fig. 1 Schematic representation of the end-tethered weak polyampholyte layer. The polymer layer consists of diblock polyelectrolytes end-grafted to a solid surface. The monomers, colored blue, are acidic in nature, meaning upon dissociation, they acquire a negative charge. The monomers, colored red, are basic in nature, being positively charged in their associated state. The monomers of acid-group carrying blocks and base-group carrying blocks are referred to as A and B monomers, respectively.

2 Theoretical Approach

The system consists of N_P copolymers, comprising monomers of type A and B, permanently end-tethered to an uncharged planar surface of area A. The polymers are in contact with an aqueous solution of a given pH and NaCl salt concentration, which is assumed to be completely dissociated. Thus, the solution reservoir consists of water molecules, cations (Na^+) and anions (Cl^-) as well as protons (H^+) and hydroxyl ions (OH^-). Different copolymer sequences have been considered by varying the lengths of each block as well as the total numbers of blocks in a chain. These sequences are denoted by $(A_xB_y)_n$. The blocks of components A and B carry oppositely charged dissociable monomers, termed acidic (A) and basic (B) monomers. Depending on the system we are studying, either all monomers or a fraction of the monomers of a block can be chargeable. In the case that only a fraction of the block is chargeable, the uncharged monomers and charged monomers of that block are assumed to be chemically identical except for their charge. Thus, non-electrostatically they interact with the solvent in the same way.

The total Helmholtz free energy is the sum of a number of different contributions, namely,

$$F = -TS_{\text{conf}} - TS_{\text{mix}} + E_{\text{VdW}} + E_{\text{rep}} + E_{\text{elec}} + F_{\text{chem}}, \qquad (1)$$

where the first three terms represent the conformational entropy of the polymer chains, the mixing entropy of all mobile species, the non-electrostatic Van der Waals interactions between the monomers, respectively. The following term describes the steric repulsion between all species. The subsequent terms are the electrostatic energy and the chemical free energy associated with the chemical equilibrium of the acidic and basic monomers, respectively. Below we present the free energy contribution in their expanded form.

The first term, the conformational entropy of the polymer chains, takes the form

$$-\frac{S_{\text{conf}}}{k_B} = \sum_{j=1}^{N_P}\sum_{\alpha} P(\alpha, j)\ln(P(\alpha, j)). \qquad (2)$$

Here, $P(\alpha, j)$ is the probability of finding an end-tethered polymer chain in the conformation α located at grafting point j. A polymer conformation is defined by the positions of all monomers of the polymer chain. The probability distribution function or pdf is the central quantity in the molecular theory because any thermodynamic and structural properties related to the polymers can be calculated from this probability distribution function. Assuming lateral homogeneity, meaning that quantities such as the polymer, solvent, and ion densities, vary only in the direction perpendicular to the surface, the conformational entropy reduces to

$$-\frac{S_{\text{conf}}}{k_B A} = \sigma_P \sum_{\alpha} P(\alpha)\ln P(\alpha). \qquad (3)$$

Here, σ_P corresponds to the surface coverage. This surface density is the number of chains per unit area and equal to N_P/A. In the current work, we have considered a planar geometry though extension to other geometries such as cylindrical and spherical ones is straightforward and involves only changes in the spatial discretization of the volume elements to take into account the curvature. From this point onward, for brevity, we present the equations only in the three-dimensional form since switching between 1D and 3D is straightforward.

Given the pdf, the local average monomer volume fraction is equal to

$$\langle\phi_i(\mathbf{r})\rangle = v_i\langle\rho_i(\mathbf{r})\rangle = v_i\sum_{j=1}^{N_P}\sum_{\alpha} P(\alpha, j)n_i(\alpha, j; \mathbf{r}). \qquad (4)$$

Here, $n_i(\alpha, j; \mathbf{r})\mathrm{d}^3\mathbf{r}$ is the number of monomers of type i located within the volume element $\mathbf{r}, \mathbf{r} + \mathrm{d}^3\mathbf{r}$ of the αth conformation that is end-tethered at the jth graft position and v_i is volume of monomer of type i.

The second free energy contribution corresponds to the mixing entropy of all mobile species and is given by

$$-\frac{S_{\text{mix}}}{k_B} = \sum_{\gamma}\int d^3\mathbf{r}\rho_\gamma(\mathbf{r})(\ln(\rho_\gamma(\mathbf{r})v_w) - 1), \qquad (5)$$

wherein index γ runs over all mobile species, which are water, Na^+, Cl^-, H^+ and OH^-. v_w is the volume of water and used as the unit of volume.

The third term represents the (effective) Van der Waals interaction energy between the monomers

$$E_{\text{VdW}} = \sum_a\sum_b -\frac{\varepsilon_{ab}}{2}\int\int g_{ab}(|\mathbf{r} - \mathbf{r'}|)\langle\rho_a(r)\rangle\langle\rho_b(r)\rangle d^3\mathbf{r}d^3\mathbf{r'}. \qquad (6)$$

Here, the indices a and b run over all monomer types. ε_{ab} corresponds to the effective strength of the Van der Waals attraction between monomer a and b. It controls the solvent quality and

$\varepsilon_{ab} = 0$ represents good solvent condition for monomers; $g_{ab}(\mathbf{r})$, which is proportional to $1/r^6$, is a distance dependent function reflecting the position dependent nature of the Van der Waals attractions. The precise mathematical form of $g_{ab}(\mathbf{r})$ can be found in electronic supporting information (ESI).

The term E_{rep} represents the steric repulsion between all species. They are modeled as excluded volume interactions. The intrachain interactions are considered exactly during chain conformation generation, while intermolecular excluded volume interactions are accounted for by assuming that the system is incompressible at every position

$$\langle\phi_A(r)\rangle + \langle\phi_B(r)\rangle + \sum_{\gamma}\phi_\gamma(r) = 1. \tag{7}$$

These volume constraints are enforced through the use of Lagrange multipliers. The fifth free energy contribution describes the electrostatic energy functional, which is given by

$$E_{\text{elec}} = \int d^3\mathbf{r}\Big[\langle\rho_q(\mathbf{r})\rangle\psi(\mathbf{r}) - \frac{1}{2}\varepsilon_o\varepsilon_r(\mathbf{r})\big(\nabla\psi\big)^2\Big], \tag{8}$$

where, ε_o is the vacuum permittivity and $\varepsilon_r(r)$ the relative dielectric constant of the medium. Here, we assume ε_r to be position independent and equal to the dielectric constant of water (78.5). In above equation $\psi(r)$ corresponds to the electrostatic potential and $\langle\rho_q(\mathbf{r})\rangle$ is the charge number density, which is given by

$$\begin{aligned}\langle\rho_q(\mathbf{r})\rangle = &-ef_{A^-}(\mathbf{r})\langle\rho_A^{dis}(\mathbf{r})\rangle + ef_{BH^+}(\mathbf{r})\langle\rho_B^{dis}(\mathbf{r})\rangle \\ &+ \sum_{i=Na^+,Cl^-,H^+,OH^-} ez_i\rho_i(\mathbf{r}),\end{aligned} \tag{9}$$

where z_i corresponds to the valence of the ions and $\langle\rho_A^{dis}(\mathbf{r})\rangle$ and $\langle\rho_B^{dis}(\mathbf{r})\rangle$ are the local number densities of the A and B monomers that are chargeable.

$$\langle\rho_i^{dis}(\mathbf{r})\rangle = \sum_{j=1}^{N_P}\sum_{\alpha}P(\alpha,j)n_i^{dis}(\alpha,j;\mathbf{r}). \tag{10}$$

These two densities depend on the specific sequence of the polymer as reflecting in $n_i^{dis}(\alpha,j;\mathbf{r})\mathrm{d}^3\mathbf{r}$, which is the number of chargeable monomers, cf with definition of Eq. 4. In the equation of the charge density, $f_{A^-}(\mathbf{r})$ corresponds to the local degree of deprotonation of the acidic monomer, while $f_{BH^+}(\mathbf{r})$ denotes the local degree of protonation of the basic monomer.

Next, F_{chem} represents the free energy associated with the acid-base equilibrium of weakly acidic ($\mathrm{AH} \rightleftharpoons \mathrm{A^-} + \mathrm{H^+}$) and weakly basic ($\mathrm{BH^+} \rightleftharpoons \mathrm{B} + \mathrm{H^+}$) monomers. The chemical free energy is given by

$$\begin{aligned}\beta F_{\text{chem}} = \int\Bigg[&\langle\rho_A^{dis}(\mathbf{r})\rangle\Big[f_{A^-}(\mathbf{r})\left(\ln f_{A^-}(\mathbf{r}) + \beta\mu_{A^-}^{\ominus}\right) + (1-f_{A^-}(\mathbf{r}))\\ &\left(\ln(1-f_{A^-}(\mathbf{r})) + \beta\mu_{AH}^{\ominus}\right)\Big] + \langle\rho_B^{dis}(\mathbf{r})\rangle\Big[f_{BH^+}(\mathbf{r})\left(\ln f_{BH^+}(\mathbf{r}) + \beta\mu_{BH^+}^{\ominus}\right)\\ &+ (1-f_{BH^+}(\mathbf{r}))\left(\ln(1-f_{BH^+}(\mathbf{r})) + \beta\mu_B^{\ominus}\right)\Big] + \sum_{i=H^+,OH^-}\beta\mu_i^{\ominus}\rho_i(\mathbf{r})\Bigg]d^3\mathbf{r}.\end{aligned} \tag{11}$$

, where $\beta = 1/(k_BT)$. The first and third terms in the above expression correspond to the mixing entropy of dissociated and undissociated states of the acidic monomers while the second and fourth term describe the internal free energy of the dissociated and undissociated states. These internal free energy contributions are expressed in terms of their standard chemical potentials ($\mu_i^{\ominus}$). The fifth through the eighth term describes similar chemical contributions related to the basic monomer. F_{chem} also includes the standard chemical potentials of the protons and hydroxyl ions, associated with the self-ionization reaction of water.

The above free energy is minimized under the constraints of local incompressibility. This along with the fact that the system is assumed to be in equilibrium with a bath of $\mathrm{H^+}$, $\mathrm{OH^-}$, $\mathrm{Na^+}$, $\mathrm{Cl^-}$ and water requires the usage of a semi-grand canonical ensemble. This results in following grand potential of the system:

$$\begin{aligned}\beta W = &\beta F + \int\beta\pi(\mathbf{r})\Big[\langle\phi_A(\mathbf{r})\rangle + \langle\phi_B(\mathbf{r})\rangle + \sum_{\gamma}\phi_\gamma(\mathbf{r}) - 1\Big]d^3\mathbf{r}\\ &-\beta\mu_{\mathrm{Na^+}}\int\rho_{\mathrm{Na^+}}(\mathbf{r})d^3\mathbf{r} - \beta\mu_{\mathrm{Cl^-}}\int\rho_{\mathrm{Cl^-}}(\mathbf{r})d^3\mathbf{r}\\ &-\beta\mu_{H^+}\int\Big[\rho_{H^+}(\mathbf{r}) + (1-f_{A^-}(\mathbf{r}))\langle\rho_A^{dis}(\mathbf{r})\rangle + f_{BH^+}(\mathbf{r})\langle\rho_B^{diss}(\mathbf{r})\rangle\Big]d^3\mathbf{r}\\ &-\beta\mu_{OH^-}\int\rho_{\mathrm{OH^-}}(\mathbf{r})\,d^3\mathbf{r}.\end{aligned} \tag{12}$$

W is minimized with respect to $P(\alpha,j)$, $f_{A^-}(\mathbf{r})$, $f_{BH^+}(\mathbf{r})$, and $\rho_\gamma(\mathbf{r})$ to yield explicit expressions for the density profiles, the polymer probability distribution function, and the fraction of charged acidic and basic monomers. The resulting polymer probability distribution function is given by

$$\begin{aligned}P(\alpha,j) = &\frac{1}{q_j}\exp\Big(\sum_a\sum_b\int\int\beta\varepsilon_{ab}\,g_{ab}(|\mathbf{r}-\mathbf{r'}|)n_a(\alpha,j;\mathbf{r})\langle\phi_b(\mathbf{r'})\rangle d^3\mathbf{r}\\ &d^3\mathbf{r'}\Big)\times\exp\Big(-\beta\int d^3\mathbf{r}\pi(\mathbf{r})[v_An_A(\alpha,j;\mathbf{r}) + v_Bn_B(\alpha,j,\mathbf{r})]\Big)\\ &\times\exp\Big(-\int d^3\mathbf{r}\,n_A^{dis}(\alpha,j;\mathbf{r})(\ln f_{A^-}(\mathbf{r}) - \beta e\psi(\mathbf{r}))\\ &\times\exp\Big(-\int d^3\mathbf{r}\,n_B^{dis}(\alpha,j;\mathbf{r})(\ln f_{BH^+}(\mathbf{r}) + \beta e\psi(\mathbf{r})),\end{aligned} \tag{13}$$

Notice that the probability of a chain conformation contains contributions from Van der Waals, electrostatic, excluded volume, and acid-base equilibria interactions of both positively and negatively charged groups. $\pi(\mathbf{r})$ is the Lagrange multiplier that imposes the incompressibility constraint and q_j is the normalization factor for the jth graft ensuring that the probability distribution function is properly normalized.

Minimization of W with respect to the fraction of charged monomers yields

$$\frac{f_{A^-}(\mathbf{r})}{1-f_{A^-}(\mathbf{r})} = K_a^{A,\ominus}\frac{\exp(-\beta\pi(\mathbf{r})v_w)}{\phi_{H^+}(\mathbf{r})}, \tag{14}$$

$$\frac{f_{BH^+}(\mathbf{r})}{1-f_{BH^+}(\mathbf{r})} = \frac{\phi_{H^+}(\mathbf{r})}{K_a^{B,\ominus}\exp(-\beta\pi(\mathbf{r})v_w)}. \quad (15)$$

In the above expressions, $K_a^{A,\ominus} = \exp(-\Delta G_a^{A,\ominus}) = \exp(-\beta(\mu_{A^-}^{\ominus} + \mu_{H^+}^{\ominus} - \mu_{AH}^{\ominus}))$ and $K_a^{B,\ominus} = \exp(-\Delta G_a^{B,\ominus}) = \exp(-\beta(\mu_B^{\ominus} + \mu_{H^+}^{o} - \mu_{BH^+}^{\ominus}))$ are the equilibrium constants of reactions $AH \rightleftharpoons A^- + H^+$ and $BH^+ \rightleftharpoons B + H^+$, respectively. These constants are related to the experimental equilibrium constants K_a^A and K_a^B by $K_a^{i,\ominus} = CK_a^i$ where $C = 1/(N_a v_w)$ is a constant that ensures consistency of units and N_a Avogadro's number. Here we like to draw attention to the fact that both the equilibrium constant of the acid as well as the base are dissociation constants.

Extremization of the free energy functional with respect to $\psi(\mathbf{r})$ results in the well-known Poisson equation for electrostatics, which along with the expressions for densities can be found in the supplementary material and Refs.[33,34]. The expressions for the volume fractions, the dissociation profiles, and the electrostatic potential result in a set of non-linear equations that have three unknowns, namely, (i) the electrostatic potential ($\psi(\mathbf{r})$), (ii) the Lagrange multipliers ($\pi(\mathbf{r})$), and (iii) the monomer volume fraction ($\langle\phi_i(\mathbf{r})\rangle$). These integro-differential equations are then discretized and solved numerically[47]. The inputs needed to solve the equations are the reservoir pH and salt concentration, the polymer dissociation constants K_a^A and K_a^B, the distribution of polymer grafting points on the surface or the surface coverage for 3D and 1D calculations, respectively and a set of polymer conformations. In the current work, a set of 10^6 polymer conformations, generated using a rotational isomeric model, are used for each grafting point. Further details on the chain model including its segment length as well as the numerical discretization can be found in the ESI as well as Refs.[33,45]. Additionally, in our study, we have considered symmetric A and B monomers with respect to their volume ($v_A = v_B = 0.11\text{nm}^{-3}$). The sizes of positive and negative salt ions have also been made equal($v_{Na^+} = v_{Cl^-} = 0.035\text{nm}^{-3}$). The volume of solvent or water is $v_w = 0.03\text{nm}^{-3}$. The volumes of H^+ and OH^- ions have been set equal to v_w. The cell size is $\delta = 0.5$ nm.

3 Results and Discussion

3.1 pH dependent dissociation behavior of monomers

To characterize the charging of weak polyelectrolyte layers, it is convenient to consider the average degree of charge arising from the deprotonated acidic monomers and protonated basic monomers. The average degrees of charge of the acidic and basic group of end-tethered polyampholytes equal the total number of acidic and basic monomers that is charged divided by the total number of acidic and basic monomers, respectively. They are obtained by the integration of the position dependent degree of dissociation and association respectively and are given by

$$\langle f_i\rangle = \frac{\int dz f_i(z)\langle\rho_i^{dis}(z)\rangle}{\int dz\langle\rho_i^{dis}(z)\rangle}. \quad (16)$$

, where i is A^- or BH^+.

Before explaining the charging of end-tethered polyampholytes, we briefly review the charging behavior of polyacids and polybases. The inset of Fig. 2 presents the average degree of dissociation of monomers of an end-tethered polyacid layer. It shows that the degree of charging is uniformly decreased as compared to the degree of dissociation of a single acidic monomer in a dilute solution. With decreasing salt concentration, the degree of charging decreases further. This behavior can be understood as follows. The concentration of monomers is high inside a polyelectrolyte layer. This results in a large electrostatic repulsion when these monomers acquire charge as the pH increases. To mitigate this unfavorable electrostatic repulsion, the system uses a few mechanisms. First, it can bring more counterions into the brush to increase electrostatic screening. This process of confining counterions is accompanied by a loss of translational entropy of the counterions. Second, the polymer chain molecules can stretch and thereby reduce intra-chain electrostatic repulsions. However, chain stretching is ineffective in negating electrostatic repulsion between nearest neighbor monomers. Also, chain stretching results in a reduction of the conformation entropy of chains. Thus, chain stretching is, like counterion confinement, 'free energy'-wise unfavorable. A third type of response involves reducing the actual number of charges by shifting the acid-base equilibrium towards the uncharged state. To do this, the system needs to perform chemical work.

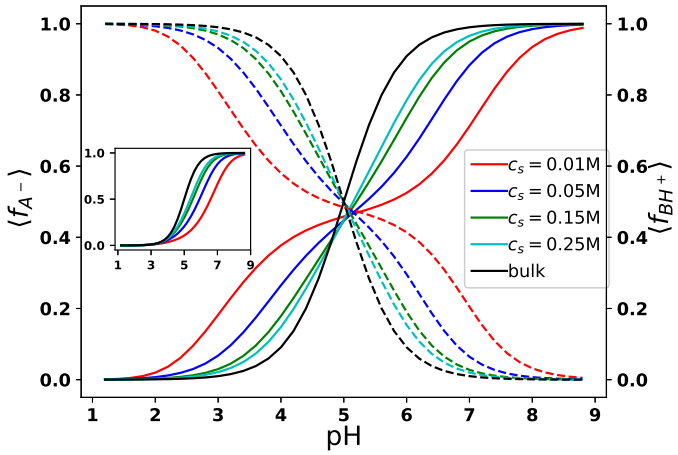

Fig. 2 The average degrees of charge fraction of A and B monomers in $A_{20}B_{20}$ block copolymer as a function of pH for different bulk salt concentrations. All monomers of both blocks are dissociable. The grafting density, σ_P, is 0.10 nm^{-2}. The solid lines and the dashed lines correspond to acidic and basic monomers, respectively.

The first two mechanisms apply to both weak and strong polyelectrolytes while the last mechanism occurs only for weak polyelectrolytes. Charge regulation by shifting the acid-base equilibrium causes the degree of charge of the polyacids to be always less than that of an isolated acidic monomer in solution. Salt ions screen the electrostatic repulsion between charged monomers. Thus a reduction in salt concentration would result in more electrostatic repulsion, which is negated by further lowering the degree of dissociation of the acidic monomers[34,43]. Thus, with decreasing salt concentration, the degree of charge of the end-tethered polyacids drops. These trends are clearly recognizable in the inset of Fig. 2. A polybase's response to pH is opposite to that

of a polyacid because a base chemically favors the neutral state at high pH and the charged state at low pH. The salt response of a layer of polybases is identical. However, for end-tethered polyampholytes that contain both acidic and basic groups, dramatically different trends emerge.

Fig. 2 depicts the average degree of dissociation of both acidic and basic monomers of an end-tethered $A_{20}B_{20}$ block copolymer for various salt concentrations and a fixed surface coverage of $\sigma_P = 0.10\ \mathrm{nm}^{-2}$. Here, the acid dissociation constants of A and B, both, have a value of $pK_a^A = pK_a^B = pK_a = 5$. Hence, one would anticipate that the acidic monomers would be mostly charged for pH values well above 5, while the reverse would be true for basic monomers, i.e, they would be mostly uncharged. Indeed, the degree of dissociation of the acidic monomers, $\langle f_{A^-} \rangle$, decreases with decreasing salt concentration for pH values above 5. However, in contrast to the homopolymer case, the behavior of the basic monomers is completely reversed. When the pH is above pK_a, the basic monomers acquire charge and salt reduction leads to an increase in the charge of the B monomers. For pH values below pK_a, the reverse behavior can be observed. Namely, the acidic monomers become charged and their degree of deprotonation increases with decreasing salt concentration while the basic monomer's fraction of charge drops with decreasing salt concentration. Also noteworthy is the presence of three inflection points, instead of one, in the dissociation curves at low salt concentration. The difference in response to salt points to additional charge regulation mechanisms for polyampholytes that are absent for pure polyacids or polybases.

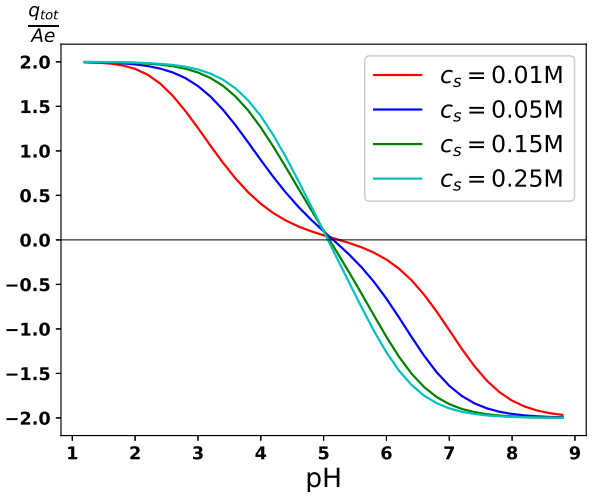

Fig. 3 The variation of the total charge per unit area on the polymer $A_{20}B_{20}$ with pH. The curves correspond to the same system as Fig. 2

To understand the cause of this charging behavior, we present in Fig. 3 the total polymer charge per unit area of the system as a function of pH for various salt concentrations. First, the figure shows that the polyelectrolyte layer has a net positive charge when the pH is less than pK_a and net negative for pH values above pK_a. For $pH \sim pK_a$, the polyelectrolyte layer is overall uncharged. Second, over the entire pH range, decreasing the salt concentration leads to a reduction of the amount of charge.

At low pH values, the brush has a net positive charge. This is because, chemically, the basic monomers would like to acquire positive charges ($pH < pK_a$) while the acidic monomers would like to remain in its neutral, protonated state. Therefore, because of the net positive charge, the system experiences a net electrostatic repulsion. To reduce this unfavorable repulsion the polyelectrolyte responds in the following manner. First, it increases the dissociation of oppositely charged acidic monomer. The chemical equilibrium of the acidic monomers is shifted upward towards the charged state as compared to the bulk solution equilibrium. This process involves chemical work. However, this is offset by the increased electrostatic attraction between the basic and acidic monomers, which reduces the overall electrostatic repulsive energy. Second, concomitant with the increasing charge of the acidic monomers, the basic monomers discharge, i.e., decrease their degree of dissociation. This results in fewer charged basic monomers, which reduces the electrostatic repulsion between like charges. Thus charge regulation of both base and acids established a new chemical equilibrium in the polyampholyte layer that reduces the amount of charge. The charge within the polymer layer is much less as compared to the amount it would carry if the acid and the base obeyed their bulk dissociation behavior. With decreasing salt concentrations, the electrostatic interactions increases in strength. To compensate for this increase, the system reduces the overall charge further. At low pH values, this results in further reduction of the charged basic monomers and an increase in the amount of charged acidic monomers. Thus, the deviation from ideal dilute solution dissociation of the acidic and basic monomers is most prominent under these conditions. At higher salt concentrations, both the electrostatic repulsion between like-charged monomers as well as the electrostatic attraction between oppositely charged monomers weaken. Consequently, the degree of dissociation will be closer to that of the dissociation of acids and bases in dilute solution.

At high pH value, the reverse happens. The polyelectrolytes carry a net negative charge, which is reduced by decreasing the number of charged acidic monomers and increasing the degree of charged basic monomers. Thus the acidic and basic monomer have reversed their role in the charge regulation process, as the most dominant contributor to the polymer charge changes from basic monomers to acidic ones. Thus, oppositely to the behavior at low pH, at high pH, the acidic monomers decrease their charge, while the basic monomers increase their charge. This reversal occurs around $pH \sim pK_a$ where the end-tethered polyampholyte has no global excess charge. Thus, the polyampholyte brush's response to a reduction in the salt concentration is essentially similar to that of a polyacid or polybase brush. Namely, across the entire pH spectrum, the overall charge of the tethered polyelectrolytes is reduced. However, the charge regulation process of the acidic and basic monomers in a polyampholyte layer is far more complex.

To stress this point further, we investigate in more detail the effect of charge regulation on the position-dependent charge and polymer distribution. So far, we have discussed the average charge of the polyampholytes and posited its behavior as arising primarily from electrostatic and chemical interactions, thereby

overlooking the influences that local monomer density can have on the charging of the polymer brush. However, there is a strong coupling between the electrostatic and chemical interaction and the conformational entropy and excluded volume interactions, which together determine the distribution of the polymer layer. With increasing surface coverage or monomer density, the monomer concentration in a polyacid or polybase layer increases and to reduce the increasing electrostatic interactions the acid-base equilibrium is shifted further towards its neutral state. Concomitantly, the brush swells or contracts as a function of pH and salt concentration. As mentioned above, the charge regulation mechanism of end-tethered polyampholytes is far more complex than that of end-tethered polyacid and polybase as does its coupling with the structure and polymer density.

To emphasize and delineate this more clearly, we plot in Figs. 4 and 5 the monomer volume fraction as well as the monomer charge profiles of a polyampholyte brush at pH values 4 and 6, respectively. Various salt concentrations are considered. The monomer charge profiles are normalized with respect to their charge valence. In the case of a homopolymer brush, the polymer volume fraction increases near the grafting surface with decreasing salt concentration causing the brush to slightly contract. Simultaneously, the total charge on the brush decreases. This corresponds to the so-called "osmotic brush" regime, as identified previously using scaling[32,48] as well as self-consistent theory approaches[49–52]. It should be noted that the contraction is small and that the general shape of the monomer profile remains unchanged. See Fig. 5 in the ESI and Refs.[33,42]. However for the diblock polyampholyte brushes, in addition to the reduction of the overall polymer charge, the density profiles change drastically in shape. At high salt concentrations, the brush is more stretched with the maximum of B monomer concentration located in the outer region for both pH values. Note that the B block is in a more extended conformation at pH 4. Likewise, the acidic and basic monomers are quite separated.

With decreasing salt concentration, the overall overlap between the A and B monomer density profiles increases: the A and B monomers move closer to each other. As the salt concentration decreases, the effect of electrostatic screening weakens and the A and B blocks would experience internally increased electrostatic repulsion. Simultaneously the electrostatic attraction between the A and B monomers increases. In response, the B monomers adopt conformations that bring the B monomers closer to the oppositely charged A monomers, which reduces the electrostatic energy. This is reflected in the maximum in the B monomer density profile that 'moves' into the A monomer region with decreasing salt concentration. Thus, the electrostatic repulsive energy is not only reduced through charge regulation but also by the polymers adopting conformations that mitigate excess electrostatic repulsion. This reduction of electrostatic repulsion occurs at the expense of conformational entropy of the polymers. Also, with the 'movement' of A and B monomers towards each other, the charged A and B monomers can act as each others counterion and less Na^+ and Cl^- ions need to be confined inside the brush. Thus less counterion confinement is required. Therefore, in a polyampholyte brush, electrostatic screening occurs not only

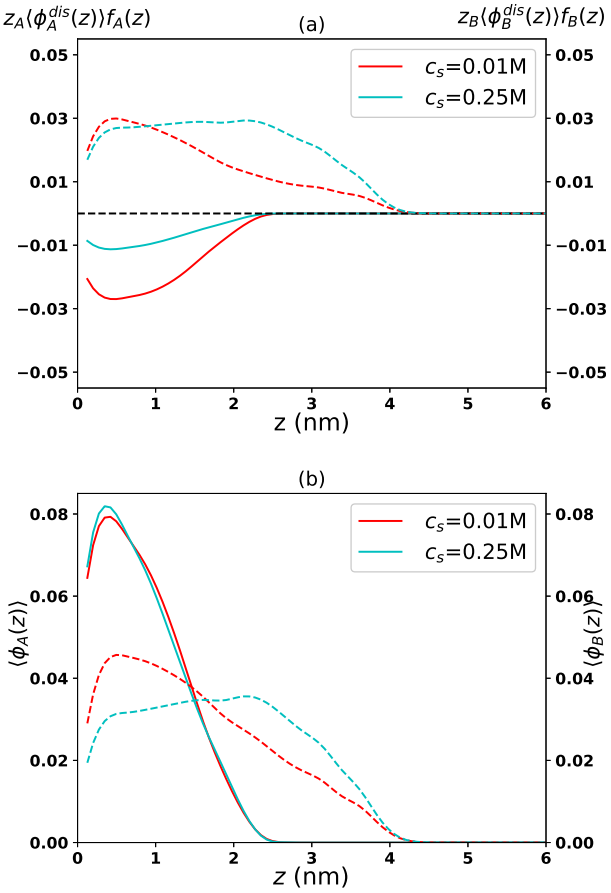

Fig. 4 The structural behavior of the polymer $A_{20}B_{20}$ at pH 4. At this pH, an isolated B monomer would be mostly charged and an A monomer would be uncharged. The lower panel shows the volume fraction profiles of the A and B monomer of a $A_{20}B_{20}$ brush. The solid and dashed line correspond to the A and B monomers, respectively. The upper panel shows the charged monomer volume fraction profiles normalized by the valence of the monomer charge. z_A and z_B denote the valencies of dissociated A and B monomers, respectively. Two salt concentrations are considered. Namely $c_s = 0.25$ M and $c_s = 0.01$ M

by counterion confinement but also through interactions between the oppositely charged monomers. Thus, the charge and structure of a layer of end-tethered weak polyampholytes is a consequence of a delicate balance between several different physical and chemical interactions that include conformational entropy, chemical free energy of the acid-base equilibrium, electrostatic interactions, osmotic pressure, and counterion confinement.

It needs to be stressed that the average charge q_{tot} and the average degree of dissociation $\langle f_{A^-}\rangle$ and $\langle f_{BH^+}\rangle$ are positional averaged quantities. The charge and the degree of dissociation, in themselves, are strongly position dependent. For example, Fig. 3 shows that the average charge q_{tot} becomes zero around $pH \sim pK_a$. This does not imply local charge neutrality. To illustrate this, we show in Fig. 6, for $pH = 5$, the position-dependent fraction of charged acidic and basic monomers alongside of the polymer volume fraction and charged density. Near the grafting surface, where the A monomers are in the majority, $f_{A^-}(z)$ is less than its corresponding bulk dissociation ($f_{A^-} = 1/2$) and the re-

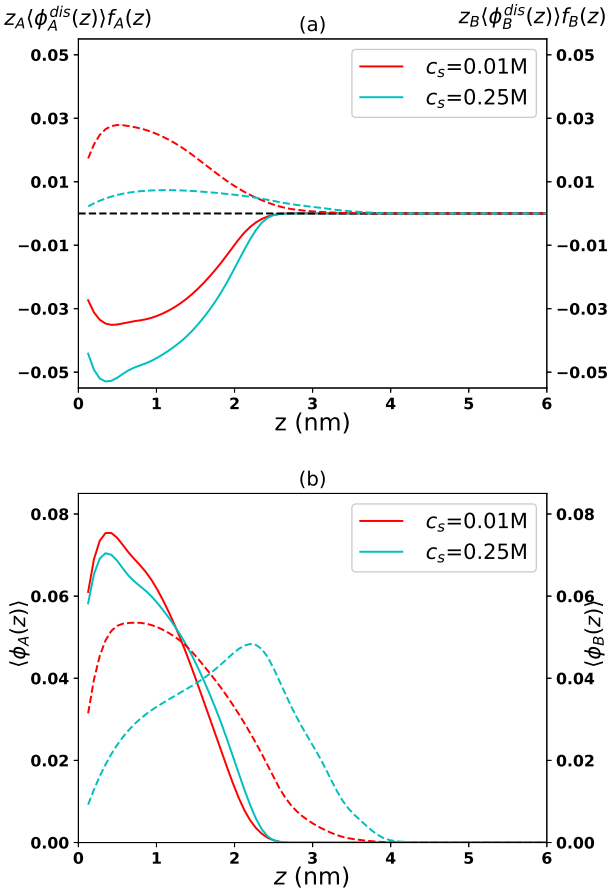

Fig. 5 The structural behavior of the polymer $A_{20}B_{20}$ at pH 6. At this pH, an isolated A monomer would be mostly charged and a B monomer would be uncharged. The lower panel shows the volume fraction profiles of the A and B monomer of a $A_{20}B_{20}$ brush. The solid and dashed lines correspond to the A and B monomers, respectively. The upper panel shows the charged monomer volume fraction profiles normalized by the valence of the monomer charge. z_A and z_B denote the valencies of dissociated A and B monomers, respectively. Two salt concentrations are considered. Namely $c_s = 0.25$ M and $c_s = 0.01$ M

verse applies to $f_{BH^+}(z)$. The basic monomers that are close to the grafting surface are more charged as expected according to to their dilute solution charge $f_{BH^+} = 1/2$).

In the outermost or distal region of the brush, there are only B monomers present. Since the B monomer density is low in the distal region of the brush, the degree of dissociation approaches that of the bases in dilute solution although only for the high salt concentration of $c_s = 0.25$ M. For the low salt concentration of $c_s = 0.01$ M, there is less electrostatic screening and the degree of charge of the basic monomer is shifted chemically to significantly lower amounts. This results in a reduction of the local electrostatic repulsion between the B monomers. Although the B monomer density is low in the distal region for the polymer layer, charge regulation still occurs in order to reduce electrostatic repulsion between to nearest neighbor monomers along the same chain. In the middle part of the brush, around $z \sim 2$nm, the A monomers gain charge up to an extent higher than the bulk solution dissociation and B monomers still carry less charge than in

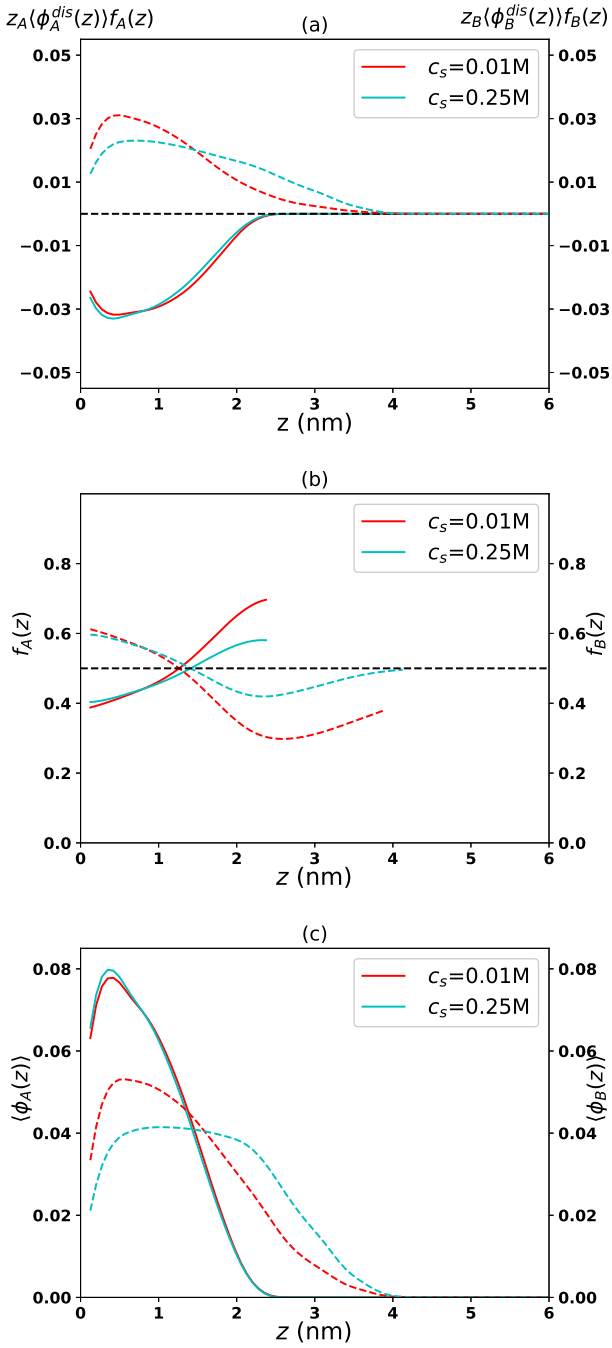

Fig. 6 The structural behavior of the polymer $A_{20}B_{20}$ at pH 5. The fraction of charged acidic and basic monomers are shown in the middle panel. The solid and dashed curves represent A and B monomers, respectively. Note that although the dissociation profiles in the theory were computed for the whole region, only regions with non-zero monomer volume fraction (>0.001) are shown. The corresponding monomer volume fraction profiles are shown in the lower panel. The top panel shows the charge profiles of A and B monomers. Salt condition identical to Figs 4 and 6

the bulk. However, in this region, as we move closer to the grafting surface, B monomers become increasingly charged, eventually reaching a degree of charging higher than that in the outermost region. Thus, the downregulation and upregulation of monomer charges are clearly distance dependent. Notice that close to the

grafting surface there is an excess amount of acidic monomers. Therefore, in the region close to the surface, the electrostatic interactions are primarily repelling and hence, downregulation of the charge of the acidic monomers occurs as compared to the solution charge. Conversely, the basic monomers undergo upregulation, but there are far less basic monomers close to the surface (a factor of around 2 at $c_s = 0.25$ M which decreases to 1.5 for $c_s = 0.01$ M see Fig 6(c)). Thus, close to the surface ($z < 1$ nm), the total charge is dominated by the charge of the acidic monomers and hence its overall charge is negative.

In the distal region, the situation is reversed and there is an excess amount of basic monomers and the overall charge is positive. Also, the basic monomer in the distal region downregulates their charge. In the intermediate region where there is considerable intermixing of monomers, both A and B monomers have more charges than in regions where they are in the majority. This results in the pattern as observed in the top panel (Fig. 6 (a)), which shows the total charge of the A and B monomers separately as a function of distance.

Also noteworthy is the fact that the effect of salt on the acid and base (charge) distribution is asymmetric. Reduction the salt concentration affects volume fraction and charge distribution of the B-monomer much more strongly than the volume fraction and charge distribution of the A monomers. As argued before, the B monomer charge, $z_B\langle\phi_B(z)\rangle f_B(z)$ decreases upon salt reduction in the outer region and decreases in the inner region, at $pH = 5$. Simultaneously, with the charge regulation, the tethered polymer undergoes conformational changes that bring the A and B more close together. Clearly, the outer block, i.e the B monomers can much easier effect these changes than the anchored A block. Hence the asymmetric response.

Finally, at $pH = 5$ the acidic and basic monomers undergo both, depending on their location, up and downregulation of their charge. However, for pH values away from the pK_a, only one type of charge regulation for a particular type of monomer dominates across the whole extent of the brush. This means the acidic and basic monomer either up or downregulate their charge. For example, in Figs. 5 (a) and 4 (a), it can be seen that at $pH = 4$, with decreasing salt concentration, the B monomers discharge while the A monomers gain charge. The reverse occurs for a pH value equal to 6.

The dissociation behavior of monomers depends not only on pH, salt concentration, and grafting density but also on the monomer sequence, the asymmetry in charge fraction as well as length for both blocks. To that end, we determine the degree of dissociation of monomers for different B-block lengths at a constant A-block length keeping the number of charged groups constant. We find that decreasing the upper block length leads to a slight yet visible increase in both $\langle f_{A^-}\rangle$ and $\langle f_{BH^+}\rangle$. Similarly, increasing the number of blocks in the chain also increases the degree of dissociation of both monomers. Thirdly, when the fractions of chargeable monomers in two blocks are different, the isoelectric point(pH corresponding to zero net charge of the polymer) shifts away from the pK_a of monomers in solution. These observations are illustrated graphically as well as explained in terms of the conformational entropy of the chain and the imbalance in charged species in sections 2.1, 2.2 and 2.3 in the ESI.

An interesting consequence of the different degrees of charging of acid and base monomers inside the polymer brush from the bulk degrees of charging of their isolated monomers is that the local proton concentration inside the brush will be different. For a pure polyacid layer, this results in an increase in the local proton concentration or equivalently a decrease in the local position dependent pH ($-\log_{10}([H^+](z))$)[33,42,45]. For a pure polybase layer, the opposite happens and the local pH increases. For a two-component brush, the behavior is different. The local proton concentrations for a $A_{20}B_{20}$ brush for different bulk pH values can be found in section 2.5 of ESI. It is seen that at $pH > pK_a$, the local pH inside the brush will be less than the bulk pH while the reverse behavior is seen at $pH < pK_a$. This means the local pH, for most part, is governed by the acidic monomer at high pH values and basic monomer at low pH values. In other words, the monomer with higher dissociation fraction at the bulk pH in question decides the local pH inside the brush. Around pK_a, a simultaneous decrease and increase in local pH is observed since both monomers are equally charged. The size of the shift in the local pH compared to the bulk pH is also strongly coupled with the salt concentration. For example, at $pH = 6$, for 250 mM salt concentration, one observes both an increase and a decrease in the local pH inside the polymer-rich region while for 10mM, only a decrease is observed.

3.2 Structural changes as a function of pH

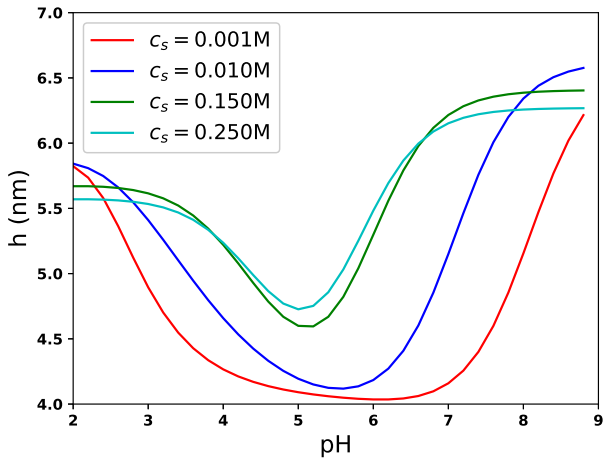

Fig. 7 The brush height as a function of pH at various salt concentrations. The grafting density corresponds to $\sigma_P = 0.10$ nm^{-2}.

Figs. 4, through 5 demonstrate that a polyampholyte layer undergoes quite drastic structural changes as a function of pH and salt concentration. To summarize these structural changes, we present in Figure 7 the height of the layer as function of pH for various salt concentrations. The height is defined as follows

$$h = 2\int dz z\langle\phi_p(z)\rangle / \int dz\langle\phi_p(z)\rangle, \tag{17}$$

and it is a measure of the thickness of the polymer layer. At

low pH, the height of the layer increases, i.e., the layer swells, with decreasing salt concentration. For low pH values, the basic monomers are charged while most acidic ones are uncharged and one of the modes by which the system mitigates the unfavorable electrostatic repulsion, is to stretch the chains, which results in swelling of the layer. Similarly, at high pH values, the acidic monomers acquire charge and the basic monomers are uncharged and the layer swells as well. Observe that the swelling of the brush as a function of pH and salt concentration is non-monotonic. Non-monotonic swelling as a function of salt concentration, but not as a function of pH, has also been observed for pure polyacids numerically[42], as well as predicted based on scaling theories[1,48,53].

In the pH-range of $4 \lesssim pH \lesssim 6$, we observe that the brush shrinks rather than swells upon salt reduction. As argued before, the polymers use, besides charge regulation and counterion confinement, also structural reorganization as a mechanism to reduce excess electrostatic repulsions. The polymer chains adopt conformations that bring the oppositely charged A and B blocks closer together and the brush shrinks.

Notice that the layer does not respond symmetrically to changes in pH. For example, at $pH = 2$ the layer swells monotonically on salt reduction in the range of salt concentration considered, whereas at $pH = 8$ the thickness changes non-monotonically. This asymmetric response is caused by the fact the polymer is grafted to the surface with its acidic block. We note that the above trend also persists qualitatively when only a fraction of the monomers are chargeable. A similar plot, for the case where only half of the monomers are chargeable, can be found in ESI.

3.3 The interplay between the solvent quality and pH

In the previous section, we investigated the chemical state and structural properties of end-tethered polyampholytes, for good solvent conditions. Reduction of the solvent quality, i.e., increasing the Van der Waals attraction between monomers, leads to a higher polymer density within the polymer brush. This can result in a collapse of the polymer layer and the possibility of microphase separation in poor solvent.

Here, we demonstrate that the degree of charge of end-tethered weak polyampholyte is sensitively coupled to the local monomer density. Since the solvent quality affects the polymer density, it will also influence the charge within the end-tethered polyelectrolytes. Before investigating the potential of microphase separation, we first focus upon the coupling between Van der Waals interaction, which controls the solvent quality, and the chemical state of charge of the polymer layer.

Fig. 8 shows the average degree of charge of the acidic and basic monomer as a function of pH for various degrees of solvent affinity for a lateral homogeneous polymer layer. Since the parameter space is huge for the studied system, we limit ourselves to the case where only the upper B-block is poor to the solvent. Fig. 8 shows the solvent quality results in a reduction of both $\langle f_{A^-} \rangle$ and $\langle f_{BH^+} \rangle$ across the entire pH range. The parameter ε_{BB} measures the solvent quality or effective Van der Waals attraction between the B monomers. Here $\varepsilon_{BB} = 0$ corresponds to good solvent conditions. As ε_{BB} increases, the upper B-block tries to avoid the solvent and increase the B monomer density within the layer. In contrast to the case of decreasing salt concentration, here decreasing the solvent quality reduces the charge of both the acidic and basic monomers, which reduces the overall charge. Here, in addition to the electrostatic attraction between the oppositely charged monomers, the electrostatic repulsion between the charged B monomers would be high as the B monomer density is increased in order to avoid the solvent. Chemically, at both low and high pH, the basic monomers respond to this increase in electrostatic repulsion among the B monomers by shifting the chemical equilibrium to its uncharged state. At low pH value, the acidic monomer still increases its charge but its upregulation decreases with increasing poor solvent quality since there are less charged bases to favor the charging of acids.

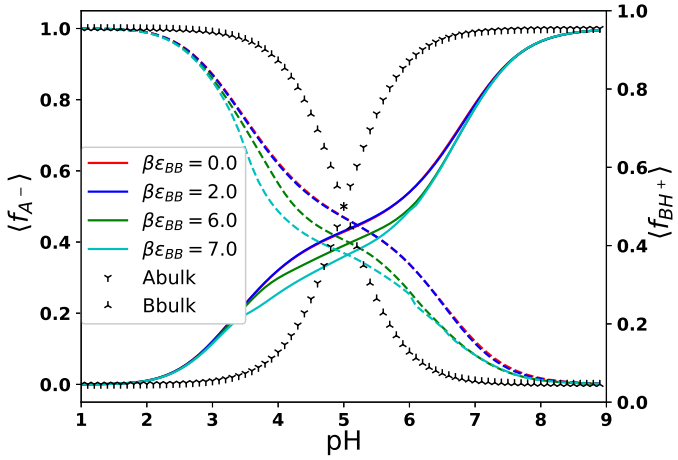

Fig. 8 The average degrees of charge fraction of A and B monomers in $A_{20}B_{20}$ block copolymer as a function of pH for different affinities of the solvent towards B block. The grafting density, σ_P, is 0.10 nm^{-2} and the salt concentration 0.01 M. The solid lines and the dashed lines correspond to acidic and basic monomers, respectively.

A similar effect is at play at a higher pH. However, above $pH >$ 7, the degree of charge of the acidic monomers is not influenced anymore by the solvent quality of the B monomers. Thus here again, like for low pH, the electrostatic repulsive energy between like charges prevails over the inter-block electrostatic attraction. Note, the basic monomer still upregulates the charge as compared to their bulk degree of charge but the upregulation decreases with increasing poor solvent quality. In summary, increases in poor solvent quality of the B monomers result in a decrease of charge of both the basic and aid monomers over the whole pH-spectrum.

Another manifestation of this interplay between the solvent quality and electrostatics is the dependence of structural behavior of the brush on pH under poor solvent conditions. In prior works on homopolymer polyelectrolyte brushes[45], the collapse and structure formation of the brush at different pH values was found to have a monotonic dependence on the bulk pH. For example, a polyacid brush collapses more readily on making the solvent quality poor at low pH than at high pH. The scenario in

the two-component brush can be expected to be different due to the presence of two types of charges.

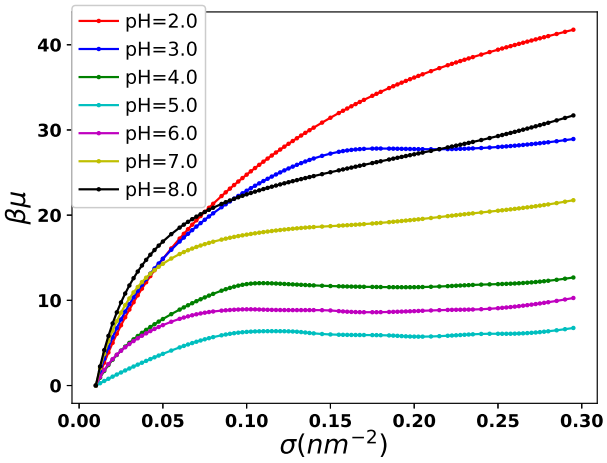

Fig. 9 Chemical potential of the polymer $A_{20}B_{20}$ as a function of surface coverage at various pH values. The salt concentration is 0.01 M. The above plots were generated for $\beta\varepsilon_{BB} = 6.0$. Here, 50 percent of both A and B monomers are dissociable.

Here, to investigate the possibility of collapse and structure formation of the brush, we examine the chemical potential of the polyelectrolytes for laterally homogeneous brushes. Fig. 9 shows the chemical potential as a function of grafting density for a poor solvent condition given by $\beta\varepsilon_{BB} = 6$ while the graph for good solvent conditions ($\beta\varepsilon_{BB} = 0$) is provided in ESI. If the slope of the chemical potential with respect to the grafting density becomes negative, the system would spontaneously phase separate into a region of higher grafting density and a region of lower grafting density. Thus, a negative slope in the μ_P vs σ curve is a measure of the system's proclivity to lateral phase separation. Note that this happens if the chains are laterally mobile. However, since here the chains are irreversibly end-grafted to the surface and therefore, lack translational freedom, phase separation into a homogeneous region of lower and higher surface coverage cannot occur. Instead we posit that microphase separation can occur. Thus, the above criterion is not sufficient to describe the onset of instability of the homogeneous brush. Instead, we take a negative slope of chemical potential to be a signature of possible phase separation and/or microphase separation. Indeed, for good solvent conditions, the chemical potential increases monotonically as a function of surface coverage for all pH values. This corroborates both our intuition and past calculations of polyacid brushes and neutral brushes that demonstrated that in good solvent the homogeneous brush is stable[33,45].

With increasing ε_{BB} (compare Fig. 9 and Fig. 10 in ESI), the μ_P versus σ curves changes from monotonically increasing to non-monotonically increasing in shape, suggesting the possibility of structure formation. Notice that chemical potential increasing monotonically with increasing grafting density for $pH = 2$ and $pH = 8$. For intermediary pH values, the chemical potential varies non-monotonically. At $pH = 2$, the basic monomers are highly charged and the electrostatic repulsion can overcome the Van der Waals attraction between the B monomers and prevent collapse and structure formation of the polymer layer. This scenario is similar to that of weak polyacid brushes in poor solvent at high pH values. This is further supported by the fact the onset of instability for a similar neutral diblock copolymer brush occurs at around $\beta\varepsilon_{BB} = 5$. This implies that the Van der Waals attraction is just sufficient to overcome the loss of conformational entropy and osmotic pressure of the system to cause collapse. As pH increases, the B monomers become less charged. Therefore, the electrostatic repulsion of the basic monomers can be overwhelmed by the Van der Waals attraction between the basic monomers. Consequently, the B layer collapses and microphase separation of the basic monomers ensues. At $pH = 8$, the chemical potential is monotonic again. This would suggest the following scenario. Namely, the (almost neutral) basic monomers collapse but remain lateral homogeneous, prevented from lateral structure formation because of the attachment to the A block that due to its high charge. However, a second and more likely scenario, confirmed by 3d calculations, is also possible. Namely, collapse and lateral structure formation of the basic monomers on top of a homogeneous layer of acidic monomers. This scenario cannot be captured by the μ_P versus σ curves since a homogeneous A layer would imply there is no driving force to vary the local grafting density. Hence, the shape of the chemical potential does not provide enough information to identify which possibility is more likely.

To identify the morphology that occurs and see if suggested structure formation as indicated by the 1D calculations really happens, we performed three dimensional calculations of the brush at different pH values and solvent qualities. Since the numerical solution is sensitive to the initial guess, we impose a microstructured pattern of interest in the calculation and then gradually remove the bias. Details of the biasing protocol can be found in the ESI. We consider three candidate morphologies, namely, micelles, lamellae, and homogeneous structures, and compare the free energy of the system to determine the most stable structure.

A hexagonal grafting pattern with a surface coverage of $0.1283 nm^{-2}$ is considered. For good solvent conditions, we confirm that the homogeneous brush is the most stable structure. Reduction of the solvent quality at $pH = 8$ and a salt concentration of $c_s = 0.01M$ result for $\beta\varepsilon_{BB} = 4.5$ in a morphological transition for a homogeneous layer to a micellar phase. This equilibrium structure consists of micelles formed by the B blocks located onto and partially submerged within a homogeneous A layer. Fig. 10 shows this equilibrium three dimensional pattern obtained at $\beta\varepsilon_{BB} = 6$. The cross-sectional density maps of the B monomers shown in panels (c) and (d) reveal that these micelles are fully spherical in shape and have considerable penetration into the A layer. Observe also that the volume fraction of the B-monomers within the micelles is quite high, up to 0.7. The volume fraction of the A layer is, in comparison, much lower and at maximum 0.3. This difference is a reflection of the fact that the acidic monomers are mostly charged and the basic monomers are mostly uncharged for the given pH value.

Keeping the solvent quality constant at $\beta\varepsilon_{BB} = 6.0$ but chang-

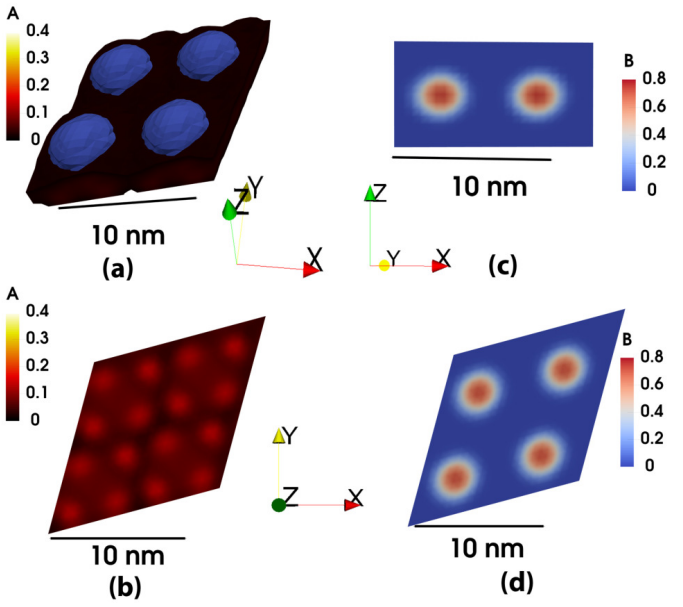

Fig. 10 Results of three dimensional calculations at pH=8 for $A_{20}B_{20}$ polymer at $\beta\varepsilon_{BB} = 6.0$. The corresponding grafting density equals 0.1283 nm^{-2}. The salt concentration is 0.01 M. Here, 50 percent of both A and B monomers are dissociable. The scales in the figure are in nanometer. The top left panel shows the three dimensional view of the microstructure. The pattern was generated by plotting the iso-density surfaces with volume fraction 0.02 or more for both A and B. Since the internal structure of the brush cannot be deciphered from this plot, we also present density maps on slices cut through the microstructure at different locations. The bottom two panels show the monomer density maps for A and B individually on cross-sectional planes cut parallel to the grafting surface. The left panel is taken at z=1.0 nm. The layer is found to be homogeneous. The circular regions represent the grafting points. The bottom right panel shows the B monomer density map of the cut at z=3.0 nm. It is clear from the circular patterns that B monomers form spherical micelles. This is confirmed by the top right panel, which maps the density of B monomers on the vertical plane passing through two adjacent micelles.

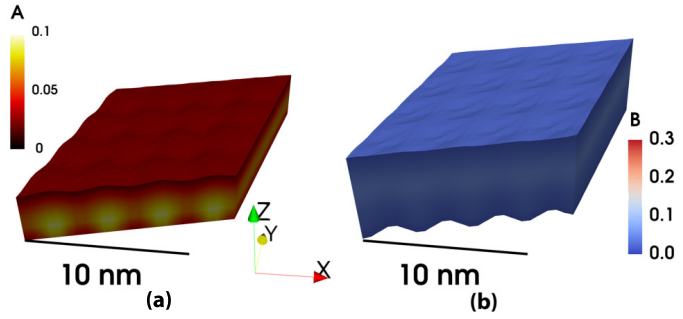

Fig. 11 Results of three dimensional calculations at pH=3 for $A_{20}B_{20}$ polymer at $\beta\varepsilon_{BB} = 6.0$. The corresponding grafting density is 0.1283 nm^{-2}. The salt concentration is 0.01 M. Here, 50 percent of both A and B monomers are dissociable. The pattern was generated by plotting the iso-density surfaces with volume fraction 0.02 or more for both A and B. Both (a) and (b) were generated from the same camera view.

ing the pH reveals that micelles formed by B blocks are the equilibrium structure at high and intermediate pH value till $pH = 4$. At lower pH values, the micellar pattern gives way to a homogeneous structure, shown in Fig. 11, as the B monomers acquire positive charges For $pH < 3$, we are unable to extract any morphological information since our calculations do not converge under such conditions. Similar structures are found for the higher salt concentration of $c_s = 0.10M$. We observed a similar morphological structural transition occurring from homogeneous layer at low pH values to a micellar phase at higher pH values. Additionally, we also find from 3D calculations that the degree of dissociation values at all pH values are lower within the collapsed structures than in homogeneous states under good solvent conditions for both monomers. For instance, for good solvent conditions ($\beta\varepsilon_{BB} = 0$), at pH=6, $\langle f_{A^-} \rangle$ and $\langle f_{BH^+} \rangle$ are 0.51 and 0.34, respectively. When the solvent becomes poor ($\beta\varepsilon_{BB} = 6.0$), these values reduce to 0.44 and 0.20, respectively. This is in line with Fig. 8, from 1D calculations, which predicts a decrease for the degree of dissociation for both monomers with decreasing solvent quality.

We also investigate the structure of the brush having poor solvent conditions for both basic as well as the acidic monomer. We found that at $pH = 3$, the acidic monomers form a lamellar striped phase with considerable surface modulations. This structure is different from traditional stripes seen in polymer brushes in that there are density inhomogeneities (undulations) within the lamellae along their axes, see Fig. 12 (a) and (b). The basic top monomers follow the topology of the acid structure, forming a cover around the A layer (shown in (c) and (d)) and filling the gap between two lamellae. In order to determine the role of electrostatics in this morphology, we ran 3D calculations for uncharged grafted chains under the same conditions. The results are shown in Fig. 13. It is seen that without charge, the collapse of monomers is more pronounced and the connectivity between rod-like features formed by A monomers improved. In the charged case, the electrostatic repulsion between collapsed same charged monomers resists a strong collapse to prevent the local build up of charges. Another difference is that the upper block collapses separately into cylinders of B monomers on top of the bottom A layer and unlike the charged case, these cylinders no longer follow the topology of the bottom block. This is due to the lack of electrostatic interactions, which has the effect of spreading the monomers apart. This explains why in the charged system, the upper layer covers the lower one. The other noteworthy feature of the charged system's microstructure is the considerable penetration of B monomers into the A layer, which shows in the cross-sectional map of B densities in 12 (d). For the uncharged system, in Fig.13, the cross-sectional map of the A monomers is shown at a height of z =0.5 nm above the grafting surface,like the density maps shown in Fig. 12. The cross-sectional density map for the corresponding B monomers at z=0.5 nm has zero density and is therefore is not shown here. Instead, the density map in 13 (c) is shown for z=1.5 nm. At higher pH values, for the charged system, the micellar B phase occurring on top of a homogeneous A phase reemerged (not shown here because it is similar to Fig. 10). However, the A phase is thinner in the case where two blocks are poor than in the case where only B block is poor.

Finally, around pH 5, the system has both negative and positive charges as both the acidic and basic monomers are partially

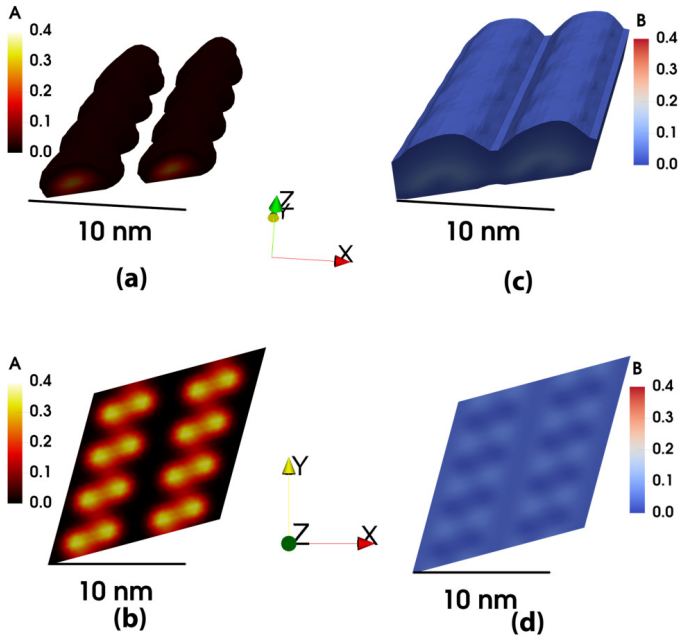

Fig. 12 Results of three dimensional calculations at pH=3 for $A_{20}B_{20}$ polymer at $\beta\varepsilon_{AA} = \beta\varepsilon_{BB} = 6.0$. $\beta\varepsilon_{AB} = \frac{\beta}{2}\sqrt{\varepsilon_{AA}\varepsilon_{BB}}$ The corresponding grafting density is 0.1283 nm^{-2}. The salt concentration is 0.01 M. The fractions of dissociable monomers in both A and B blocks are 0.5. The scales in the figure are in nanometer. The top left panel shows the three dimensional view of the A monomers and the top right panel shows a similar view of the B monomers. The patterns were generated by plotting the iso-density surfaces with volume fraction 0.02 or more for both A and B. The bottom left panel shows the A monomer density map on a cross-sectional plane cut parallel to the grafting surface at z=0.5 nm. The bottom right panel shows the B monomer density map of the cut at z=0.5 nm.

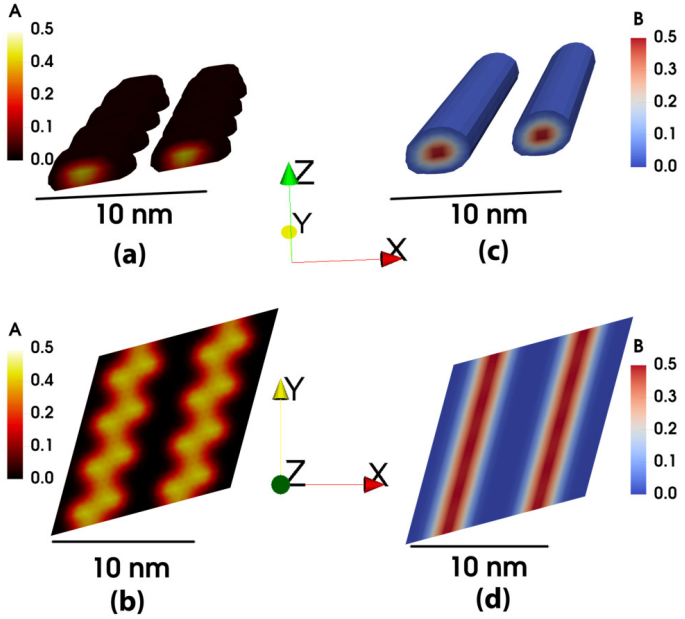

Fig. 13 Results of three dimensional calculations for neutral $A_{20}B_{20}$ polymer at $\beta\varepsilon_{AA} = \beta\varepsilon_{BB} = 6.0$. $\beta\varepsilon_{AB} = \frac{\beta}{2}\sqrt{\varepsilon_{AA}\varepsilon_{BB}}$. The corresponding grafting density is 0.1283 nm^{-2}. The scales in the figure are in nanometer. The top two panels show the three dimensional view of the brush. The patterns were generated by plotting the iso-density surfaces with volume fraction 0.02 or more for both A and B. The bottom left panel shows the A monomer density map on a cross-sectional plane cut parallel to the grafting surface at z=0.5 nm. The bottom right panel shows the B monomer density map of the cut at z=1.5 nm.

charged. This could result in novel more complex structures. We tried to obtain those structures by seeding the initial guess of the numerical solver by either a homogeneous, lamellae or micelles structures. Novel structures were not found. However, instead it turned out to be challenging to obtain any numerical solutions for pHs values around 5. Frequently, we were not able to obtain a converged solution at all. This could be related to fact that we lack appropriate candidates structures. We reserve this numerical challenging project for a future investigation.

4 Conclusions

Here we have investigated, through a molecular theory, the chemical state and structural proprieties of end-tethered diblock polyampholytes comprising acidic and basic monomers with equal acid dissociation constants (pK_a). For $pH \lesssim pK_a$, salt reduction increases the degree of deprotonation or charge of the acidic monomers and decreases the protonation or charge of the basic monomers. The reverse happens for $pH \gtrsim pK_a$. This behavior is opposite to the charging of end-grafted homo-polyelectrolytes, where salt reduction results in a decrease in the degree of charge of monomers at all pHs. Overall, the charge regulation of polyampholytes brushes causes the net charge to decrease as the salt concentration is reduced. The charge regulation results from a complex balance between chemical and physical interactions, which involve among others electrostatic and excluded volume interaction, and conformational entropy of the polymers.

The charge of weak polyacid layers is primarily determined through a balance between charge regulation, which shifts the acid-base equilibrium, counter-ion confinement, and loss of conformational entropy by chain stretching. For end-tethered diblock polyelectrolytes that consist of both acidic and basic monomers an additional effect is important. Namely, large conformational changes of the polymer chain that 'move" the upper block of basic monomers towards the lower block consisting of acidic monomers. This results in an unusual non-monotonic structural response as a function of pH and salt. At low and high pH values the end-tethered polyampholytes layer swells as the salt concentration is reduced, while at intermediate pH values the brush shrinks when the salt concentration is decreased. The importance of conformational entropy is also reflected in the fact that the degree of dissociation of the acidic and basic monomers is influenced by the number of blocks($A_{20}B_{20}$, $(AB)_{20}$, etc) as well as the relative block lengths.

Another noteworthy observation is the distance-dependent charge regulating effect near $pH \sim pK_a$, where the brush is overall electroneutral. Under these conditions, decreasing the salt concentration decreases the number of charged basic monomers in the outer part of the brush, where they are in an overwhelming majority, and increases it in the inner part of the brush, where

they are surrounded by oppositely charged acidic monomers. The acidic monomers follow a reverse position dependent pattern. For pHs away from the pK_a, only one of these effects dominates across the entire brush. Either the acidic monomers decrease their charge and the basic monomers increase their charge or vice versa depending on the pH value.

We also find strong solvent quality effects on the chemical and structural state of the brush. With decreasing the solvent quality of the basic monomers, both the acidic and basic monomers uncharge. For sufficiently strong Van der Waals attraction, pattern formation occurs. For poor solvent quality of the basic monomer (B), a morphological transition from a homogeneous B layer to a micellar B phase on top of a homogeneous A phase occurs as pH is increased. Similarly, for poor solvent condition of both blocks, a lamellar pattern of acidic monomers with longitudinal compositional undulations engulfed by a layer of basic monomers occurs at low pH values, while a micellar B phase on top of a homogeneous A layer is observed at high pH values. Future directions include finding more appropriate candidate structures that may occur at intermediate pH values.

We point out that our Molecular theory, in spite of including many molecular details of the polyelectrolyte, still is an approximate theory, which can potentially be improved upon. First, the electrostatic interactions are considered at a mean-field level, hence neglecting short-range electrostatic correlations[54–58]. These correlations are important and capable of collapsing strongly charged polyelectrolytes in good solvent conditions if the Bjerrum length, $l_B = e^2/(4\pi\varepsilon_o\varepsilon_r k_B T)$, times the polyelectrolyte linear charge density, $1/b$, where b is the distance between charges, is greater than one (i.e., $l_B/b > 1$)[59]; here, e is the elementary charge, ε_o is the permittivity of vacuum, ε_r is the relative permittivity and $k_B T$ is the thermal energy. This has been corroborated by simulations that account for a decrease in local ε_r with increasing polyelectrolyte concentration[60]. Short-range electrostatic correlations are also important in multivalent ion conditions due to an enhancement of the ionic correlations[61], or due to ion bridges[62]. In the present work, the counterions are monovalent and the Bjerrum length is 0.7 nm and the distance between adjacent monomers is 0.35 nm so $l_B/b = 2$ only when the blocks are fully charged. However, by setting the fraction of chargeable monomers to 0.5, (meaning inserting additional neutral monomers) so $l_B/b = 1$, the mean-field assumption is justified, which we have done for poor solvent conditions. Note that at low salt concentrations, the counterions gain substantial entropy when they are free in the solution, instead of forming ion pairs or clusters of correlated ions and monomers. Moreover, for the fully chargeable case, since clustering of acid and base groups will not be significant for most pH values as the opposite charges are located on different blocks, we believe short-range electrostatic correlations will not affect our results significantly. We reserve the potential improvement to include many body effects resulting from electrostatic correlations in the theory when applicable for future work.

Secondly, the dielectric environment in the brush is assumed to be homogeneous, which, strictly speaking, does not accurately reflect the dielectric environment of the actual brush. The effect of dielectric function on the chemical state of polyacid brushes was found to be small for good solvent conditions and moderately dense brushes[34]. However, the effect of dielectric heterogeneity can become prominent for high local polymer concentrations, which can occur under poor solvent conditions. A model incorporating the position-dependent dielectric constant[34] as well as surface polarization effects[63], which affect the polymer conformation in confinement[64] , would be a refinement of our current work. It would also be interesting to see the effect of dielectric mismatch between two blocks on the dissociation and collapse behavior of the brush.

To the best of our knowledge, the simultaneous upregulation and downregulation of charge of acidic and basic monomers by salt in end-tethered block polyampholyte layers has not been systemically explored in the past. Past theoretical investigations that considered charge regulation of weak polyampholytes usually consider a more complex setting of e.g., protein (a polyampholyte) adsorption onto a polyelectrolyte gel or brush[65] or charge regulation of a virus capsid[66]. There the presence of multiple different types of acids and bases on the protein complicated and obscured the clear the up and down regulation pattern demonstrated here. Therefore, these current results are helpful to gain a deeper understanding complex phenomena such as protein adsorption. Also, the unusual charging and the non-monotonic structural response as a function of salt and pH can have potential applications involving polymer tethered nano-channels for ion pumping or rectification[67,68]. In a wider sense, our results demonstrate that weak polyampholyte layers have a much richer phase behavior than polyacid and polybase layers, which expands the physical and chemical parameter space to control and rationally design stimuli-responsive materials. In summary, our work provides guidelines and insights for further investigations, both experimental as well as theoretical, into the morphological behavior of end-tethered weak polyampholytes.

Conflicts of interest

There are no conflicts to declare.

Acknowledgements

D.P, M.O.d.l.C. and R.J.N thank the support from the Center for Bio-Inspired Energy Science, an Energy Frontier Research Center funded by the U.S. Department of Energy (DOE), Office of Science, Basic Energy Sciences (BES), under Award # DE-SC0000989 and the Northwestern University Center of Computation and Theory of Soft Materials. I.S acknowledges support from NSF, Div. of Chem. Bioeng. Env. and Transp. Sys. 1833214. We acknowledge the computational support of Sherman Fairchild Foundation. D.P and R.J.N thank Dr. Kai Huang for insightful discussions concerning the biasing method and Dr. Mario Tagliazucchi for useful discussions.

Notes and references

1 P. Pincus, *Macromolecules*, 1991, **24**, 2912–2919.
2 B. Zhao and W. J. Brittain, *Progress in Polymer Science*, 2000, **25**, 677–710.

3 I. Luzinov, S. Minko and V. V. Tsukruk, *Progress in Polymer Science*, 2004, **29**, 635–698.

4 J. Klein, E. Kumacheva, D. Mahalu, D. Perahia and L. J. Fetters, *Nature*, 1994, **370**, 634.

5 R. A. Wright, K. Wang, J. Qu and B. Zhao, *Angewandte Chemie International Edition*, 2016, **55**, 8656–8660.

6 M. A. Cohen Stuart, W. T. Huck, J. Genzer, M. Müller, C. Ober, M. Stamm, G. B. Sukhorukov, I. Szleifer, V. V. Tsukruk, M. Urban *et al.*, *Nature materials*, 2010, **9**, 101–113.

7 J. R. Werber, C. O. Osuji and M. Elimelech, *Nature Reviews Materials*, 2016, **1**, 1–15.

8 S. P. Adiga and D. W. Brenner, *Journal of functional biomaterials*, 2012, **3**, 239–256.

9 H. Ouyang, Z. Xia and J. Zhe, *Microfluidics and nanofluidics*, 2010, **9**, 915–922.

10 H. Zhang, X. Hou, L. Zeng, F. Yang, L. Li, D. Yan, Y. Tian and L. Jiang, *Journal of the American Chemical Society*, 2013, **135**, 16102–16110.

11 B. Yameen, M. Ali, R. Neumann, W. Ensinger, W. Knoll and O. Azzaroni, *Journal of the American Chemical Society*, 2009, **131**, 2070–2071.

12 Y. Shen, Y. Zhan, J. Tang, P. Xu, P. A. Johnson, M. Radosz, E. A. Van Kirk and W. J. Murdoch, *AIChE journal*, 2008, **54**, 2979–2989.

13 M. Müllner, *Macromolecular Chemistry and Physics*, 2016, **217**, 2209–2222.

14 M. A. Borden, H. Zhang, R. J. Gillies, P. A. Dayton and K. W. Ferrara, *Biomaterials*, 2008, **29**, 597–606.

15 A. K. Gupta and M. Gupta, *Biomaterials*, 2005, **26**, 1565–1573.

16 M. Ballauff and O. Borisov, *Current Opinion in Colloid & Interface Science*, 2006, **11**, 316–323.

17 K. N. Witte, J. Hur, W. Sun, S. Kim and Y.-Y. Won, *Macromolecules*, 2008, **41**, 8960–8963.

18 R. Dong, M. Lindau and C. K. Ober, *Langmuir*, 2009, **25**, 4774–4779.

19 Y.-H. Lin, J. Teng, E. R. Zubarev, H. Shulha and V. V. Tsukruk, *Nano letters*, 2005, **5**, 491–495.

20 T. Chen, I. Amin and R. Jordan, *Chemical Society Reviews*, 2012, **41**, 3280–3296.

21 S. V. Orski, K. H. Fries, S. K. Sontag and J. Locklin, *Journal of Materials Chemistry*, 2011, **21**, 14135–14149.

22 E. B. Zhulina, C. Singh and A. C. Balazs, *Macromolecules*, 1996, **29**, 6338–6348.

23 Y. Yin, P. Sun, B. Li, T. Chen, Q. Jin, D. Ding and A.-C. Shi, *Macromolecules*, 2007, **40**, 5161–5170.

24 D. Meng and Q. Wang, *The Journal of chemical physics*, 2009, **130**, 134904.

25 R. Jiang, B. Li, Z. Wang, Y. Yin and A.-C. Shi, *Macromolecules*, 2012, **45**, 4920–4931.

26 N. Houbenov, S. Minko and M. Stamm, *Macromolecules*, 2003, **36**, 5897–5901.

27 E. Bittrich, M. Kuntzsch, K.-J. Eichhorn and P. Uhlmann, *Journal of Polymer Science Part B: Polymer Physics*, 2010, **48**, 1606–1615.

28 K. Yu and Y. Han, *Soft Matter*, 2009, **5**, 759–768.

29 D. Meng and Q. Wang, *The Journal of chemical physics*, 2011, **135**, 224904.

30 R. Israels, F. Leermakers and G. Fleer, *Macromolecules*, 1994, **27**, 3087–3093.

31 R. Israels, D. Gersappe, M. Fasolka, V. A. Roberts and A. C. Balazs, *Macromolecules*, 1994, **27**, 6679–6682.

32 R. Israels, F. Leermakers, G. J. Fleer and E. B. Zhulina, *Macromolecules*, 1994, **27**, 3249–3261.

33 R. Nap, P. Gong and I. Szleifer, *Journal of Polymer Science Part B: Polymer Physics*, 2006, **44**, 2638–2662.

34 R. J. Nap, M. Tagliazucchi and I. Szleifer, *The Journal of chemical physics*, 2014, **140**, 024910.

35 N. Shusharina and P. Linse, *The European Physical Journal E*, 2001, **6**, 147–155.

36 N. Shusharina and P. Linse, *The European Physical Journal E*, 2001, **4**, 399–402.

37 G. Fleer, M. Cohen Stuart, J. M. Scheutjens, T. Cosgrove and B. Vincent, *Polymers at interfaces*, Springer Science & Business Media, 1993.

38 M. Baratlo and H. Fazli, *Physical Review E*, 2010, **81**, 011801.

39 L.-J. Qu, X. Man, C. C. Han, D. Qiu and D. Yan, *The Journal of Physical Chemistry B*, 2012, **116**, 743–750.

40 G. S. Longo, M. O. de la Cruz and I. Szleifer, *Soft Matter*, 2012, **8**, 1344–1354.

41 I. Szleifer and M. Carignano, *Advances in chemical physics*, 1996, **94**, 165–260.

42 P. Gong, T. Wu, J. Genzer and I. Szleifer, *Macromolecules*, 2007, **40**, 8765–8773.

43 D. Wang, R. J. Nap, I. Lagzi, B. Kowalczyk, S. Han, B. A. Grzybowski and I. Szleifer, *Journal of the American Chemical Society*, 2011, **133**, 2192–2197.

44 P. Gong, J. Genzer and I. Szleifer, *Physical review letters*, 2007, **98**, 018302.

45 M. Tagliazucchi, M. O. de la Cruz and I. Szleifer, *Proceedings of the National Academy of Sciences*, 2010, **107**, 5300–5305.

46 A. Yethiraj and C. E. Woodward, *The Journal of chemical physics*, 1995, **102**, 5499–5505.

47 A. C. Hindmarsh, P. N. Brown, K. E. Grant, S. L. Lee, R. Serban, D. E. Shumaker and C. S. Woodward, *ACM Transactions on Mathematical Software (TOMS)*, 2005, **31**, 363–396.

48 E. B. Zhulina and M. Rubinstein, *Soft matter*, 2012, **8**, 9376–9383.

49 K. N. Witte, S. Kim and Y.-Y. Won, *The Journal of Physical Chemistry B*, 2009, **113**, 11076–11084.

50 O. Borisov, T. Birshtein and E. Zhulina, *Journal de Physique II*, 1991, **1**, 521–526.

51 E. Zhulina, T. Birshtein and O. Borisov, *Macromolecules*, 1995, **28**, 1491–1499.

52 Y. V. Lyatskaya, F. Leermakers, G. Fleer, E. Zhulina and T. Birshtein, *Macromolecules*, 1995, **28**, 3562–3569.

53 E. Zhulina and O. Borisov, *The Journal of chemical physics*,

1997, **107**, 5952–5967.
54 J. Jiang, V. V. Ginzburg and Z.-G. Wang, *Soft matter*, 2018, **14**, 5878–5887.
55 T. Jiang and J. Wu, *The Journal of Physical Chemistry B*, 2008, **112**, 7713–7720.
56 T. Jiang, Z. Li and J. Wu, *Macromolecules*, 2007, **40**, 334–343.
57 T. Hofmann, R. Winkler and P. Reineker, *The Journal of Chemical Physics*, 2001, **114**, 10181–10188.
58 C. E. Sing, J. W. Zwanikken and M. O. De La Cruz, *Nature materials*, 2014, **13**, 694–698.
59 P. González-Mozuelos and M. O. De la Cruz, *The Journal of chemical physics*, 1995, **103**, 3145–3157.
60 I. Nakamura and Z.-G. Wang, *Soft Matter*, 2013, **9**, 5686.
61 F. J. Solis and M. O. De La Cruz, *The Journal of Chemical Physics*, 2000, **112**, 2030–2035.
62 R. J. Nap, S. H. Park and I. Szleifer, *Soft Matter*, 2018, **14**, 2365–2378.
63 Y. Levin, *Physical review letters*, 2009, **102**, 147803.
64 T. D. Nguyen and M. Olvera de la Cruz, *ACS nano*, 2019, **13**, 9298–9305.
65 C. F. Narambuena, G. S. Longo and I. Szleifer, *Soft Matter*, 2015, **11**, 6669–6679.
66 R. J. Nap, A. L. Božič, I. Szleifer and R. Podgornik, *Biophysical journal*, 2014, **107**, 1970–1979.
67 M. Tagliazucchi, Y. Rabin and I. Szleifer, *Journal of the American Chemical Society*, 2011, **133**, 17753–17763.
68 S. Qin, H. Kai and I. Szleifer, *Unpublished*.